

Second-order topological phases protected by chiral symmetry

Ryo Okugawa,¹ Shin Hayashi,² and Takeshi Nakanishi²

¹*WPI-Advanced Institute for Materials Research (WPI-AIMR),
Tohoku University, 2-1-1, Katahira, Sendai 980-8577, Japan*

²*Mathematics for Advanced Materials-OIL, AIST, 2-1-1 Katahira, Aoba, 980-8577 Sendai, Japan*

(Dated: July 3, 2019)

We study second-order topological phases characterized by chiral symmetry in the absence of crystal symmetries. We investigate topological phase transitions of a model for the two-dimensional second-order topological insulators protected by chiral symmetry. By the theory of the phase transitions, we propose chiral-symmetric second-order topological semimetals. Various second-order topological semimetals can be obtained from the stacked two-dimensional second-order topological insulators with chiral symmetry. Moreover, we show that broken chiral symmetry allows a topological phase transition from the second-order topological semimetal to a second-order topological insulator with chiral hinge states in the three-dimensional system. We also demonstrate the second-order topological phases by using a lattice model.

I. INTRODUCTION

Higher-order topological insulators have recently drawn research interest as new topological crystalline phases^{1–30}. Unlike conventional first-order topological insulators, two-dimensional (2D) second-order topological insulators (SOTIs) have topologically protected corner states, and three-dimensional (3D) SOTIs have topological gapless modes on the hinges. In some crystalline SOTIs, the topological corner and hinge states can arise only from the nontrivial bulk topology when the lattice termination is compatible with the crystal symmetries.

The idea of the crystalline SOTIs has been extended to semimetallic phases, which are called second-order topological semimetals (SOTSMs)^{14–16,20,31}. SOTSMs have not only topological hinge states but also topological gapless nodes in the bulk and/or on the surfaces. Intriguingly, a mirror-symmetric SOTSM enables topological semimetal phases on the surfaces while the bulk gap is open³¹. The topological hinge states appear between the surface gapless points projected onto the hinges.

On the other hand, crystal symmetry is not necessarily required in order to realize SOTIs^{6–8,32–39}. If crystal symmetry is absent, the topological classification of the d -dimensional second-order topological phases is the same as that of the $(d - 1)$ -dimensional first-order topological phases in the Altland-Zirnbauer classes^{6–8,38–40}. Thus, the SOTIs in the 3D class A and the 2D class AIII are characterized by \mathbb{Z} invariants. In the 2D (3D) SOTIs without crystal symmetry, both the bulk and the edges (surfaces) determine topology of the corner (hinge) states. The SOTI phases are stable topologically as long as the bulk and the boundary are gapped even if we arbitrarily change the lattice termination^{6–8}.

However, the boundary Hamiltonian is typically complicated. Therefore, the phase diagram for search for the SOTI is difficult to explore analytically without employing crystal symmetry. Moreover, since topological phase transitions characterize topological semimetals in the momentum space, SOTSMs without crystal symmetry have

not been revealed yet.

In this work, we show various second-order topological phases protected by chiral symmetry without crystal symmetry. We discuss a simple method to construct the chiral-symmetric second-order topological phases. To do so, we develop the previous method^{38,39} for the 2D SOTI with chiral symmetry in view of the topological phase transition. From our theory, we also show different 3D SOTSMs due to chiral symmetry, and one of them is an unconventional topological semimetal which has a single gapless point on the 2D surface. Furthermore, it is found that broken chiral symmetry in SOTSMs can induce a 3D SOTI phase without any symmetry.

The paper is organized as follows. In Sec. II, we show the method for construction of the second-order topological phases due to chiral symmetry. We demonstrate the topological phases by a lattice model constructed from our method in Sec. III. Our conclusion is summarized in Sec. IV.

II. SECOND-ORDER TOPOLOGICAL PHASES CHARACTERIZED BY CHIRAL SYMMETRY

In this section, we study SOTIs and SOTSMs protected by *chiral symmetry* in terms of the bulk and edge gap-closings for the topological phase transitions. We propose simple Hamiltonians to create the second-order topological phases *without crystal symmetries*.

A. Corner states and topological invariant

First of all, we review construction of 2D SOTIs by chiral symmetry according to Ref. 38. We apply the method to 3D systems with chiral symmetry later. We consider the following bulk Hamiltonian:

$$H(\mathbf{k}) = \mathcal{H}_x(k_x) \otimes \Pi_y + 1_x \otimes \mathcal{H}_y(k_y), \quad (1)$$

where $\mathcal{H}_i(k_i)$ ($i = x, y$) are two Hermitian matrices with chiral symmetry represented as Π_i . Here, $\Pi_i^2 = 1_i$, and

1_i is the identity matrix with the same size as $\mathcal{H}_i(k_i)$. Because $\{\mathcal{H}_i, \Pi_i\} = 0$ is satisfied, the Hamiltonian in Eq. (1) has chiral symmetry $\Pi = \Pi_x \otimes \Pi_y$. In this paper, we focus on gap closing at zero energy because chiral symmetry is present. When the model is gapped at zero energy, it can be characterized by a \mathbb{Z} topological invariant given by³⁹

$$\nu_{2D} = w_x w_y, \quad (2)$$

where $w_{i=x,y}$ are conventional winding numbers for $\mathcal{H}_i(k_i)$. The expression of the winding number is given in the Appendix A. The winding numbers distinguish whether the 1D bulk Hamiltonians $\mathcal{H}_i(k_i)$ are in the first-order topological phase by chiral symmetry⁴¹⁻⁴⁴. As discussed in the next section, ν_{2D} is unchanged as long as the model is gapped at zero energy in the bulk and on the edges. The system with the nonzero ν_{2D} is a 2D SOTI with zero-energy corner states.

Indeed, the nonzero ν_{2D} indicates existence of the corner states when the edges break the translation symmetries in the x and the y directions. We consider a semi-infinite system with one corner for Eq. (1). Because k_x and k_y are separate in Eq. (1), the corner Hamiltonian can be described by two edge Hamiltonians of $\mathcal{H}_x(k_x)$ and $\mathcal{H}_y(k_y)$. We denote the edge Hamiltonians of $\mathcal{H}_i(k_i)$ as \mathcal{H}_i^{edge} . The corner Hamiltonian is represented as

$$H^{corner} = \mathcal{H}_x^{edge} \otimes \Pi_y^{edge} + 1_x^{edge} \otimes \mathcal{H}_y^{edge}. \quad (3)$$

Here, Π_y^{edge} and 1_x^{edge} are representations of the chiral symmetry and the identity matrix in the terminated system, respectively. To see topological corner states, we assume that the bulk and the edges are gapped at zero energy. If both $\mathcal{H}_x(k_x)$ and $\mathcal{H}_y(k_y)$ are topologically nontrivial, i.e. $\nu_{2D} \neq 0$, we can see the corner states with the zero energy as follows. Let ϕ_i^{zero} be one of the topological zero-energy eigenvectors of \mathcal{H}_i^{edge} at one zero-dimensional edge from the nonzero w_i . Then, we can find a zero-energy state given by $\phi_x^{zero} \otimes \phi_y^{zero}$ for H^{corner} in Eq. (3). By assumption, the zero-energy state should be a corner state. Generally, we can obtain $|\nu_{2D}| = |w_x w_y|$ topological corner states because $\mathcal{H}_{i=x,y}^{edge}$ have $|w_i|$ zero-energy modes. Thus, zero-energy corner states appear when ν_{2D} is nonzero.

B. Topological phase transitions and gap closing

To grasp the 2D SOTI, we revisit the topological phase transitions in view of the gap closing. We clarify how the topological phases for $H(\mathbf{k})$ change when we continuously deform $\mathcal{H}_i(k_i)$. In other words, we can see how the band gap necessarily closes in the bulk or the edges when ν_{2D} changes.

We assume that the system is in a trivial phase with $\nu_{2D} = 0$ to elucidate the topological phase transitions. $\mathcal{H}_x(k_x)$ and $\mathcal{H}_y(k_y)$ need to close the band gap to change

$\nu_{2D} = w_x w_y$. To begin with, we discuss the bulk gap given by Eq. (1). Because $\{\mathcal{H}_y, \Pi_y\} = 0$, the bulk Hamiltonian satisfies

$$H(\mathbf{k})^2 = \mathcal{H}_x(k_x)^2 \otimes 1_y + 1_x \otimes \mathcal{H}_y(k_y)^2. \quad (4)$$

Therefore, if and only if $\mathcal{H}_x(k_x)$ and $\mathcal{H}_y(k_y)$ take zero-valued eigenvalues at the same time, the bulk bands close the gap. This gap closing can change both w_x and w_y , and thus ν_{2D} .

By contrast, ν_{2D} can change even if $\mathcal{H}_x(k_x)$ and $\mathcal{H}_y(k_y)$ do not take zero-valued eigenvalues simultaneously. We consider a trivial phase with $(w_x, w_y) = (1, 0)$. From the above discussion, when the system enters a nontrivial phase with $(w_x, w_y) = (1, 1)$ from the trivial phase, the bulk Hamiltonian $H(\mathbf{k})$ does not close the band gap. Then, we investigate an edge normal to the x direction. Namely, we see a semi-infinite system with the edge along the y direction. Because we retain periodicity in the y direction, the edge can be described as

$$H_x^{edge}(k_y) = \mathcal{H}_x^{edge} \otimes \Pi_y + 1_x^{edge} \otimes \mathcal{H}_y(k_y). \quad (5)$$

Although $H_x^{edge}(k_y)$ satisfies the condition similar to Eq. (4), we note that $\mathcal{H}_y(k_y)$ determines gap closing on the edge because $\mathcal{H}_x(k_x)$ has the nonzero w_x . \mathcal{H}_x^{edge} has the topological zero-mode ϕ_x^{zero} now, and $\mathcal{H}_y(k_y)$ has Bloch eigenstates $\psi_{n_y}(k_y)$ with the eigenvalues $E_{n_y}(k_y)$. Therefore, an eigenvector of the $\mathcal{H}^{edge}(k_y)$ can be obtained from $\phi_x^{zero} \otimes \psi_{n_y}(k_y)$ because it satisfies

$$H_x^{edge}(k_y)[\phi_x^{zero} \otimes \psi_{n_y}(k_y)] = E_{n_y}(k_y)[\phi_x^{zero} \otimes \psi_{n_y}(k_y)]. \quad (6)$$

$\mathcal{H}_y(k_y)$ can effectively describe the edge states near zero energy thanks to the nontrivial topology of $\mathcal{H}_x(k_x)$. Hence, the gap closes on the edge when $\mathcal{H}_y(k_y)$ takes zero-valued eigenvalues.

We also analyze a topological phase transition from the phase with $(w_x, w_y) = (0, 1)$ to the phase with $(1, 1)$. In this case, we show that gap closing happens on the edge normal to the y direction. The edge Hamiltonian is

$$H_y^{edge}(k_x) = \mathcal{H}_x(k_x) \otimes \Pi_y^{edge} + 1_x \otimes \mathcal{H}_y^{edge}. \quad (7)$$

Similarly, we can obtain an eigenstate of $H_y^{edge}(k_x)$ from $\psi_{n_x}(k_x) \otimes \phi_y^{zero}$ due to the nonzero w_y . $\psi_{n_x}(k_x)$ is a Bloch function of $\mathcal{H}_x(k_x)$. We can choose ϕ_y^{zero} to satisfy $\Pi_y^{edge} \phi_y^{zero} = \pm \phi_y^{zero}$ because this state is a zero-energy mode of \mathcal{H}_y^{edge} . Therefore, the gap closes on the edge through the eigenvalues of $\mathcal{H}_x(k_x)$.

C. Construction of 3D SOTSMs and SOTIs

Hereafter, we generalize the theory about the 2D SOTI to 3D systems with chiral symmetry. Since the wavevector k_z is added to Eq. (1) in the 3D systems, the bulk Hamiltonian is given by

$$H(\mathbf{k}) = \mathcal{H}_x(k_x, k_z) \otimes \Pi_y + 1_x \otimes \mathcal{H}_y(k_y, k_z). \quad (8)$$

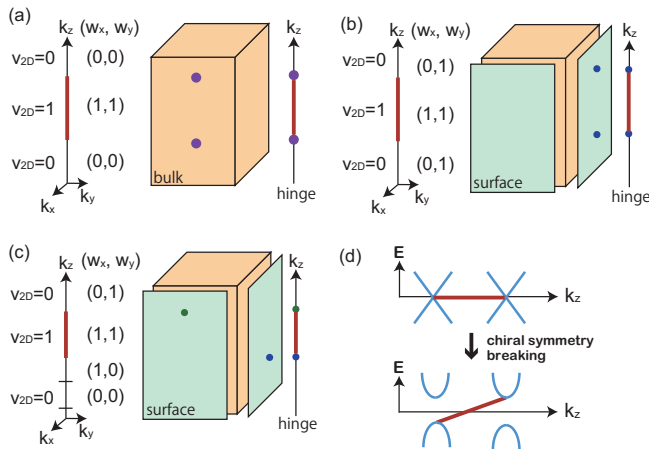


FIG. 1. (a)-(c) Schematic drawings of gapless points in the SOTSMs. The dots are the gapless points. The red lines indicate the topological hinge states. (a) The bulk gap-closings give rise to the gapless points. (b) and (c) The gapless points appear from the surface gap-closings while the bulk is insulating. The surface gap closes when $\nu_{2D}(k_z)$ changes. (d) Schematic drawing of hinge band evolution for the topological phase transition from the 3D SOTSM to the 3D SOTI.

Thus, we can regard k_z as a new parameter leading to the topological phase transition characterized by $\nu_{2D}(k_z)$. The topological phase transition can occur in the momentum space, in which gap-closing points can emerge due to the chiral symmetry for the 3D system. Therefore, the phase has the topological gap-closing points and hinge states at zero energy. As a result, we can realize a SOTSM by stacking the 2D SOTIs.

The positions of the gapless points depend on how $\mathcal{H}_x(k_x, k_z)$ and $\mathcal{H}_y(k_y, k_z)$ give rise to the topological phase transitions. Because $\nu_{2D}(k_z)$ is periodic for k_z , point nodes always appear in pairs. If \mathcal{H}_x and \mathcal{H}_y change the winding numbers w_x and w_y simultaneously, a semimetallic phase emerges in the bulk, as shown in Fig. 1(a). The system shows zero-energy hinge states between the nodes projected onto the hinges because of the nonzero $\nu_{2D}(k_z)$. For example, the gapless node appears when (w_x, w_y) changes from $(0, 0)$ to $(1, 1)$ in the 3D momentum space.

By contrast, the system can have gapless points on the surfaces. There are two types of the topological phase transitions by the change in k_z , which results in surface topological semimetals. We consider the first type where gapless points appear on the same surface. In this type, one of w_x and w_y changes in the momentum space while the other one is fixed to a nonzero value, for instance [Fig. 1(b)].

In the second type, we can obtain gapless points on the different surfaces. The point nodes can be found when w_x and w_y change in the momentum space. We note that this surface topological semimetal is unique to the 3D systems because 2D bulk topological semimetals necessarily have topological point nodes in pairs in

the momentum space^{44–48}. As an example, each surface can have a single gapless point if (w_x, w_y) changes as $(0, 1) \rightarrow (0, 0) \rightarrow (1, 0) \rightarrow (1, 1) \rightarrow (0, 1)$, as illustrated in Fig. 1(c). In both of the two types, topological hinge states appear at the zero energy between the gapless points.

Next, we break chiral symmetry in the 3D SOTSM with the gapless points on the surfaces. The gap opens at the point nodes because the symmetry protection is absent. Hence, we can discuss a surface Chern insulator due to massive Dirac cones^{33,34,37,49}. In the specific case, we can easily diagnose existence of the gapless hinge states (see the Appendix B). Typically, if the pairs become gapped by broken chiral symmetry, they can contribute to the surface Chern numbers. The chiral hinge states appear between the gapped surfaces on the trivial bulk. Consequently, the system can show the 3D SOTI phase without symmetry [Fig. 1(d)].

III. MODEL

We study a lattice model to demonstrate the second-order topological phases realized by chiral symmetry, and confirm our theory in the previous section. The lattice model is constructed from the Su-Schrieffer-Heeger (SSH) model.

A. 2D SOTI model

We construct second-order topological phases and the Hamiltonian by the general method from Eq. (1). We

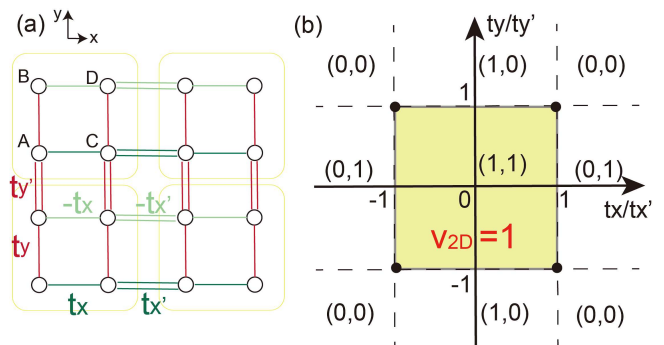


FIG. 2. (a) Schematic drawing of the 2D model for the 2D SOTI. The unit cell consists of four sublattices. (b) Phase diagram of the 2D model. The yellow shaded region represents the topological phase. When (w_x, w_y) gives the nonzero ν_{2D} , the gap closing occurs. The dots on the phase boundary represent the bulk gap-closings.

study a 2D tight-binding model described as

$$\begin{aligned}
H = & \sum_{\mathbf{R}} [t_x (c_{\mathbf{R}C}^\dagger c_{\mathbf{R}A} - c_{\mathbf{R}D}^\dagger c_{\mathbf{R}B} + H.c.) \\
& + t_y (c_{\mathbf{R}B}^\dagger c_{\mathbf{R}A} + c_{\mathbf{R}D}^\dagger c_{\mathbf{R}C} + H.c.) \\
& + t'_x (c_{\mathbf{R}+\hat{x}A}^\dagger c_{\mathbf{R}C} - c_{\mathbf{R}+\hat{x}B}^\dagger c_{\mathbf{R}D} + H.c.) \\
& + t'_y (c_{\mathbf{R}+\hat{y}A}^\dagger c_{\mathbf{R}B} + c_{\mathbf{R}+\hat{y}C}^\dagger c_{\mathbf{R}D} + H.c.)], \quad (9)
\end{aligned}$$

where \hat{x} and \hat{y} are the unit vectors in the x and y directions, respectively. t_x, t'_x, t_y and t'_y are hopping parameters (See Fig. 2(a)). We set the lattice constants to unity. The Hamiltonian in the momentum space is

$$\begin{aligned}
H(\mathbf{k}) = & [(t_x + t'_x \cos k_x)\tau_x + t'_x \sin k_x \tau_y] \otimes \sigma_z \\
& + \tau_0 \otimes [(t_y + t'_y \cos k_y)\sigma_x + t'_y \sin k_y \sigma_y], \quad (10)
\end{aligned}$$

where $\sigma_{x,y,z}$ and $\tau_{x,y,z}$ are Pauli matrices acting on the sublattices, and σ_0 and τ_0 are the identity matrices. The energy eigenvalues are

$$E(\mathbf{k}) = \pm \sqrt{\sum_{i=x,y} [(t_i + t'_i \cos k_i)^2 + (t'_i \sin k_i)^2]}. \quad (11)$$

This model actually consists of the two SSH models represented by

$$\mathcal{H}_{j=x,y}(k_j) = \begin{pmatrix} 0 & t_j + t'_j e^{-ik_j} \\ t_j + t'_j e^{ik_j} & 0 \end{pmatrix}, \quad (12)$$

and the chiral symmetry is given by

$$\Pi_{x,y} = \begin{pmatrix} 1 & 0 \\ 0 & -1 \end{pmatrix}. \quad (13)$$

Thus, this 2D model⁵⁰ has chiral symmetry $\Pi = \tau_z \otimes \sigma_z$.

The topological invariant ν_{2D} can be calculated from the winding numbers w_j for $\mathcal{H}_j(k_j)$. They are given by

$$w_j = \begin{cases} 1 & |t_j/t'_j| < 1 \\ 0 & |t_j/t'_j| > 1 \end{cases}. \quad (14)$$

Hence, we can obtain the phase diagram for the 2D model from Eq. (2) [Fig. 2 (b)].

B. Stacked SOTI model

We stack the 2D SOTI model to demonstrate 3D second-order topological phases. While we preserve the chiral symmetry, we introduce terms depending on k_z . The dependence on k_z is determined by how the 2D SOTIs are stacked in the z direction.

Firstly, we add two terms $2\chi_1 \cos k_z \tau_x \otimes \sigma_z$ and $2\chi_2 \cos k_z \tau_0 \otimes \sigma_x$ to the Hamiltonian in Eq. (10). These terms effectively alter the hopping terms t_x and t_y to $t_x + 2\chi_1 \cos k_z$ and $t_y + 2\chi_2 \cos k_z$, respectively. Hence, the topological phase transition can happen in the momentum space. When $t_x + 2\chi_1 \cos k_z = \pm t'_x$ ($|t_y/t'_y| \leq 1$)

and/or $t_y + 2\chi_2 \cos k_z = \pm t'_y$ ($|t_x/t'_x| \leq 1$) can be satisfied, the k_z planes have gapless points.

Suppose that $t_x = t_y$, $t'_x = t'_y$ and $\chi_1 = \chi_2$. In the parameter region, we can obtain a SOTSM with the bulk gapless points. If the parameters change as the red arrow in Fig. 3(a), two fourfold-degenerate points appear at $(k_x, k_y, k_z) = (\pi, \pi, \pm \arccos \frac{t'_x - t_x}{2\chi_1})$ in the bulk. The topological hinge states also exist between the projected point nodes, as shown in Fig. 3(b).

Next, we set $\chi_2 = 0$ to see a SOTSM with gapless points on the surfaces. Since t_y is fixed, only w_x can change in the momentum space. Therefore, we can realize a SOTSM with the gapless points on the surface perpendicular to the y direction. For example, we change t_x as the green arrow in the diagram. w_x and ν_{2D} change when $t_x + 2\chi_1 \cos k_z = t'_x$. Figure 3 (c) shows the two surface nodes at $(k_x, k_z) = (\pi, \pm \arccos \frac{t'_x - t_x}{2\chi_1})$ and the zero-energy hinge states between the two points projected to the hinges.

Secondly, we add new terms $(2\eta \cos k_z + \delta t_x)\tau_x \otimes \sigma_z$ and $(2\eta \sin k_z + \delta t_y)\tau_0 \otimes \sigma_x$, instead of the previous two terms. The hopping t_x (t_y) is effectively regarded as $t_x + \delta t_x + 2\eta \cos k_z$ ($t_y + \delta t_y + 2\eta \sin k_z$). If $t'_x = t'_y$, the modified hoppings form the circle in the diagram, as depicted in Fig. 3(a). Thus, the gap closing can occur on the different surfaces when the circle encloses a phase transition point accompanied by bulk gap-closing. We assume that the circle encloses the point $t_x/t'_x = t_y/t'_y = 1$, and that $\eta/t'_x > 0$. Then, the point nodes appear at $(k_x, k_z) = (\pi, -\arccos \frac{t'_x - t_x - \delta t_x}{2\eta})$ and $(k_y, k_z) = (\pi, \pi - \arcsin \frac{t'_y - t_y - \delta t_y}{2\eta})$ on the surfaces normal to the y and the x directions, respectively [Fig. 3 (d)]. The anomalous distribution of the point nodes is allowed because the gap closings both in the bulk and on the surfaces change the hinge topology, similarly to a mirror-symmetric SOTSM³¹. To annihilate the surface point nodes, the gap should close in the bulk.

We emphasize that our Hamiltonian does not need any crystal symmetries to realize the second-order topological phases. The 2D chiral-symmetric model actually has two mirror symmetries. However, even if the mirror symmetries are broken, the SOTSM phases can survive as long as the chiral symmetry exists. We can indeed see the protection of the chiral symmetry by breaking the mirror symmetries. For example, we introduce the term $2t_{w_1} \cos k_z \tau_y \otimes \sigma_z + 2t_{w_2} \cos k_z \tau_0 \otimes \sigma_y$ for the case in Fig. 3(c). If $t_{w_{1,2}} \ll t'_{x,y}$, the topological zero-modes are stable because ν_{2D} does not change [Fig. 4 (a)].

C. SOTSMs with broken chiral symmetry

Finally, we break chiral symmetry to produce a 3D SOTI from the 3D SOTSM with the surface gapless points. By using our model, we here show that the SOTI can be realized easily from the SOTSM in Fig. 3 (c). We

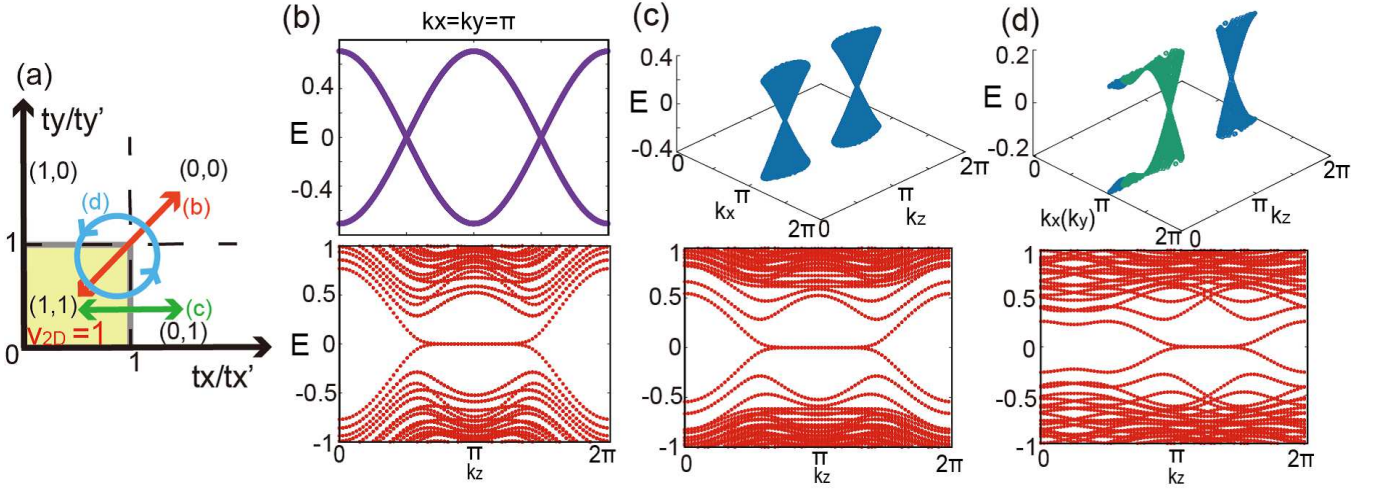


FIG. 3. (a) Trajectories of the hopping parameters in the phase diagram. We put $t'_x = t'_y = 1$ in the numerical calculations. The red (green) arrow indicates the case where $t_x = t_y = 1.0$ and $\chi_1 = \chi_2 = 0.25$ for (b) ($t_x = 1.0, t_y = 0.4, \chi_1 = 0.25$, and $\chi_2 = 0$ for (c)). The blue circle represents the change in the hopping parameters with $t_x = t_y = 0.5, \delta t_x = \delta t_y = 0.3$, and $\eta = 0.2$ for (d). (b)-(d) The upper figures show gap-closing points from the topological phase transitions, and the lower figures show the hinge bands in a regular square column with the 15×15 unit cells. In (b), the bulk bands are calculated along the line $(k_x, k_y) = (\pi, \pi)$. The bulk has the point nodes at $k_z = \pi/2$ and $3\pi/2$ on the line. The upper figure in (c) shows bands for the surfaces normal to the y direction. The surface bands have nodal points at $(k_x, k_z) = (\pi, \pi/2)$ and $(\pi, 3\pi/2)$. In (d), the blue and the green bands represent electronic structures for the surfaces normal to the y and the x directions, respectively. The gapless point in the blue (green) bands is located at $(k_x, k_z) = (\pi, 5\pi/3)$ ($(k_y, k_z) = (\pi, 5\pi/6)$).

add the perturbation $2t_m \sin k_z \tau_z \otimes \sigma_z$ in order to obtain the SOTI. Figure 4 (b) shows the gapless hinge states which originate from the zero-energy states.

To understand the topological phase transition, we investigate the surface normal to the y direction from the discussion in Sec.II B. Because \mathcal{H}_y is topologically nontrivial, the surface states considered are represented effectively as $\mathcal{H}_{\text{eff}} = (t_x + t'_x \cos k_x + 2\chi_1 \cos k_z)\tau_x + t'_x \sin k_x \tau_y + 2t_m \sin k_z \tau_z$ (see also the Appendix B). The effective Hamiltonian describes the surface Dirac points with the mass induced by the broken chiral symmetry.

We can calculate the surface Chern number from \mathcal{H}_{eff} . The effective Hamiltonian near the gapless points $\mathbf{k}^\pm \equiv (\pi, \pm \arccos \frac{t'_x - t_x}{2\chi_1})$ is given by

$$\mathcal{H}_{\text{eff}}^\pm(\mathbf{q}) = -(2\chi_1 \sin k_z^\pm)q_z \tau_x - t'_x q_x \tau_y + 2t_m \sin k_z^\pm \tau_z, \quad (15)$$

where $\mathbf{q} = (q_x, q_z)$ is wave vector measured from \mathbf{k}^\pm . By the perturbation term, the Dirac cones at \mathbf{k}^\pm obtain the mass gap described as $2t_m \sin k_z^\pm \tau_z$. Because $\sin k_z^\pm > 0$ and $\chi_1/t'_x > 0$ in the calculation, the surface has the Chern number $\text{sgn}(t_m)$. As a result, the system becomes the SOTI phase, which is consistent with the discussion in the Appendix B.

IV. CONCLUSION AND DISCUSSION

In the present paper, we have shown that various chiral-symmetric second-order topological phases are re-

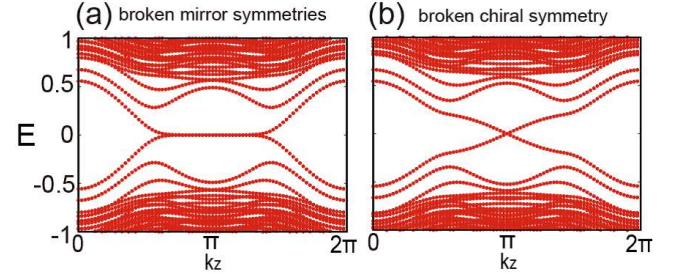


FIG. 4. The hinge bands for the case of Fig. 3 (c) with broken symmetries. (a) The zero-energy hinge states survive without the mirror symmetries after the perturbation with $t_{w_1} = t_{w_2} = 0.1$ is added. (b) The gapless chiral hinge states emerge by the perturbation with $t_m = 0.1$.

alizable without crystal symmetries. We have suggested the method to construct the second-order topological phases protected only by chiral symmetry. The theory reveals that there are several types of chiral-symmetric second-order topological semimetals in three-dimensional systems, and that the topological semimetals can be obtained from stacked two-dimensional second-order topological insulators with chiral symmetry. The zero-energy hinge states are stable topologically by chiral symmetry. Particularly, we discover a second-order topological semimetal whose surface has a single gapless point thanks to chiral symmetry. In general, this surface topological semimetal is not allowed in the two-dimensional bulk because both of the bulk and the surfaces need to

contribute topologically. It is also shown that broken chiral symmetry can yield the second-order topological insulator from the second-order topological semimetal in the three-dimensional system.

Importantly, if any Hamiltonian with chiral symmetry can be continuously deformed to Eq. (1) or (8) without the bulk and surface gap-closings, we can distinguish whether the system has nontrivial second-order topology because the band topology is unchanged. Namely, our theory is useful even though the Hamiltonian does not take the form in Eq. (1) or (8). Therefore, our proposed topological phases universally appear. Thus, our model is available for many systems whose structures are flexibly controllable, such as photonic and phononic crystals and electric circuits²⁶⁻³⁰. Additionally, second-order topological phases have been predicted in superconductors^{6-8,10,51-56}. Because of chiral symmetry, the second-order topological nodal phases suggested in our paper are expected to appear in superconductors with time-reversal symmetry.

ACKNOWLEDGMENTS

We are grateful to R. Takahashi and S. Murakami for helpful discussion. This work is supported by World Premier International Research Center Initiative (WPI), MEXT, Japan, JPSJ Grant-in-Aid Scientific Research on Innovative Areas Discrete Geometric Analysis for Materials Design (Grant No. 17H06460 and No. 17H06461), and JSPS KAKENHI Grant Number JP19K14545 and 16K05412, and JST-CREST (JPMJCR18T1).

Appendix A: Expression of the winding number

To describe the topological invariant ν_{2D} in a self-contained way, we explicitly write the winding number w for the 1D Hamiltonian with chiral symmetry. To do so, we introduce the following Q -matrix given by

$$Q(k) = 1 - 2 \sum_{E_n < 0} |\psi_n(k)\rangle \langle \psi_n(k)|, \quad (\text{A1})$$

where the sum is taken over the eigenstates $|\psi_n(k)\rangle$ below zero energy. In the basis where the chiral symmetry is diagonal, the Q -matrix can be rewritten as

$$Q(k) = \begin{pmatrix} 0 & q(k) \\ q^\dagger(k) & 0 \end{pmatrix}. \quad (\text{A2})$$

By using the off-diagonal component $q(k)$, the winding number is defined as⁴²⁻⁴⁴

$$w = \frac{i}{2\pi} \int_0^{2\pi} dk \text{Tr}[q^{-1} \partial_k q]. \quad (\text{A3})$$

The winding number w corresponds to the number of the topological edge states in the 1D chiral-symmetric system.

Appendix B: Model for chiral hinge states

In this appendix, we give a 3D Hamiltonian which shows chiral hinge states without any symmetry. The Hamiltonian is beneficial to obtain the 3D SOTI in the class A. We consider the following bulk Hamiltonian given by³⁸

$$H_A(\mathbf{k}) = \mathcal{H}_{xz}(k_x, k_z) \otimes \Pi_y + 1_x \otimes \mathcal{H}_y(k_y). \quad (\text{B1})$$

Here, $\mathcal{H}_{xz}(k_x, k_z)$ is a Hermitian matrix without symmetry, and 1_x has the same size as $\mathcal{H}_{xz}(k_x, k_z)$. $\mathcal{H}_y(k_y)$ is the chiral-symmetric Hamiltonian explained in Sec. II. We assume that the bulk and the surface gaps are open at zero energy. Because Eqs. (B1) and (1) have the same structures, we discuss the topological hinge states similarly to Sec. II by regarding $\mathcal{H}_{xz}(k_x, k_z)$ as a 2D bulk Hamiltonian. Therefore, we define a Chern number Ch_{xz} for $\mathcal{H}_{xz}(k_x, k_z)$, which gives the 1D chiral edge states ψ^{chiral} . The Chern number Ch_{xz} is defined for the bulk bands below zero energy since the origin of the energy can be shifted.

To see chiral hinge states in the 3D SOTI, we investigate the semi-infinite Hamiltonian with one hinge:

$$H_A^{hinge}(k_z) = \mathcal{H}_{xz}^{edge}(k_z) \otimes \Pi_y^{edge} + 1_x^{edge} \otimes \mathcal{H}_y^{edge}. \quad (\text{B2})$$

We maintain the translation symmetry in the z direction. In the same way as Sec. II, we can obtain topological hinge states $\psi^{chiral}(k_z) \otimes \phi^{zero}$ with the gapless dispersion if Ch_{xz} and w_y are nonzero. Thus, we can introduce a \mathbb{Z} topological invariant $I = Ch_{xz}w_y$, which characterizes the number of the gapless hinge states³⁸. Realistically, \mathcal{H}_y can depend on k_z . However, since k_z can be interpreted as a parameter in $\mathcal{H}_y(k_y)$, gapless hinge states can be detected if the model can be adiabatically deformed to Eq. (B1).

In comparison with our model in Sec. III C, \mathcal{H}_{xz} corresponds to \mathcal{H}_{eff} . The massive Dirac cones on the surface gives the nonzero Chern number $Ch_{xz} = \text{sgn}(t_m)$. As a result, we obtain the chiral hinge states from the SOTSM with the broken chiral symmetry.

¹ W. A. Benalcazar, B. A. Bernevig, and T. L. Hughes, *Science* **357**, 61 (2017).

² W. A. Benalcazar, B. A. Bernevig, and T. L. Hughes, *Phys. Rev. B* **96**, 245115 (2017).

³ Z. Song, Z. Fang, and C. Fang, *Phys. Rev. Lett.* **119**, 246402 (2017).

⁴ C. Fang and L. Fu, arXiv:1709.01929 (2017).

⁵ F. Schindler, A. M. Cook, M. G. Vergniory, Z. Wang, S. S.

- Parkin, B. A. Bernevig, and T. Neupert, *Sci. Adv.* **4**, eaat0346 (2018).
- ⁶ J. Langbehn, Y. Peng, L. Trifunovic, F. von Oppen, and P. W. Brouwer, *Phys. Rev. Lett.* **119**, 246401 (2017).
- ⁷ M. Geier, L. Trifunovic, M. Hoskam, and P. W. Brouwer, *Phys. Rev. B* **97**, 205135 (2018).
- ⁸ L. Trifunovic and P. W. Brouwer, *Phys. Rev. X* **9**, 011012 (2019).
- ⁹ E. Khalaf, H. C. Po, A. Vishwanath, and H. Watanabe, *Phys. Rev. X* **8**, 031070 (2018).
- ¹⁰ E. Khalaf, *Phys. Rev. B* **97**, 205136 (2018).
- ¹¹ A. Matsugatani and H. Watanabe, *Phys. Rev. B* **98**, 205129 (2018).
- ¹² G. van Miert and C. Ortix, *Phys. Rev. B* **98**, 081110(R) (2018).
- ¹³ S. H. Kooi, G. van Miert, and C. Ortix, *Phys. Rev. B* **98**, 245102 (2018).
- ¹⁴ Z. Wang, B. J. Wieder, J. Li, B. Yan, and B. A. Bernevig, arXiv:1806.11116.
- ¹⁵ M. Ezawa, *Phys. Rev. B* **97**, 155305 (2018).
- ¹⁶ M. Ezawa, *Phys. Rev. Lett.* **120**, 026801 (2018).
- ¹⁷ M. Ezawa, *Phys. Rev. Lett.* **121**, 116801 (2018).
- ¹⁸ M. Ezawa, *Phys. Rev. B* **97**, 241402(R) (2018).
- ¹⁹ M. Ezawa, *Phys. Rev. B* **98**, 045125 (2018).
- ²⁰ M. Ezawa, *Scientific reports* **9**, 5286 (2019).
- ²¹ T. Fukui and Y. Hatsugai, *Phys. Rev. B* **98**, 035147 (2018).
- ²² F. K. Kunst, G. van Miert, and E. J. Bergholtz, *Phys. Rev. B* **97**, 241405(R) (2018).
- ²³ S. Franca, J. van den Brink, and I. C. Fulga, *Phys. Rev. B* **98**, 201114(R) (2018).
- ²⁴ D. Călugăru, V. Juričić, and B. Roy, *Phys. Rev. B* **99**, 041301(R) (2019).
- ²⁵ F. Schindler, Z. Wang, M. G. Vergniory, A. M. Cook, A. Murani, S. Sengupta, A. Y. Kasumov, R. Deblock, S. Jeon, I. Drozdov, *et al.*, *Nat. Phys.* **14**, 918 (2018).
- ²⁶ S. Imhof, C. Berger, F. Bayer, J. Brehm, L. W. Molenkamp, T. Kiessling, F. Schindler, C. H. Lee, M. Greiter, T. Neupert, *et al.*, *Nat. Phys.* **14**, 925 (2018).
- ²⁷ M. Serra-Garcia, V. Peri, R. Süsstrunk, O. R. Bilal, T. Larsen, L. G. Villanueva, and S. D. Huber, *Nature* **555**, 342 (2018).
- ²⁸ C. W. Peterson, W. A. Benalcazar, T. L. Hughes, and G. Bahl, *Nature* **555**, 346 (2018).
- ²⁹ X. Ni, M. Weiner, A. Alù, and A. B. Khanikaev, *Nat. Mater.* **18**, 113 (2019).
- ³⁰ H. Fan, B. Xia, L. Tong, S. Zheng, and D. Yu, *Phys. Rev. Lett.* **122**, 204301 (2019).
- ³¹ M. Lin and T. L. Hughes, *Phys. Rev. B* **98**, 241103(R) (2018).
- ³² G. E. Volovik, *JETP Lett.* **91**, 201 (2010).
- ³³ M. Sitte, A. Rosch, E. Altman, and L. Fritz, *Phys. Rev. Lett.* **108**, 126807 (2012).
- ³⁴ F. Zhang, C. L. Kane, and E. J. Mele, *Phys. Rev. Lett.* **110**, 046404 (2013).
- ³⁵ K. Hashimoto, X. Wu, and T. Kimura, *Phys. Rev. B* **95**, 165443 (2017).
- ³⁶ L. Li, M. Umer, and J. Gong, *Phys. Rev. B* **98**, 205422 (2018).
- ³⁷ W. Chen and J. L. Lado, *Phys. Rev. Lett.* **122**, 016803 (2019).
- ³⁸ S. Hayashi, *Commun. Math. Phys.* **364**, 343 (2018).
- ³⁹ S. Hayashi, *Lett. Math. Phys.* (2019), 10.1007/s11005-019-01184-w.
- ⁴⁰ J. C. Y. Teo and C. L. Kane, *Phys. Rev. B* **82**, 115120 (2010).
- ⁴¹ S. Ryu and Y. Hatsugai, *Phys. Rev. Lett.* **89**, 077002 (2002).
- ⁴² A. P. Schnyder, S. Ryu, A. Furusaki, and A. W. W. Ludwig, *Phys. Rev. B* **78**, 195125 (2008).
- ⁴³ S. Ryu, A. P. Schnyder, A. Furusaki, and A. W. W. Ludwig, *New J. Phys.* **12**, 065010 (2010).
- ⁴⁴ C.-K. Chiu, J. C. Y. Teo, A. P. Schnyder, and S. Ryu, *Rev. Mod. Phys.* **88**, 035005 (2016).
- ⁴⁵ S. Matsuura, P.-Y. Chang, A. P. Schnyder, and S. Ryu, *New J. Phys.* **15**, 065001 (2013).
- ⁴⁶ Y. X. Zhao, A. P. Schnyder, and Z. D. Wang, *Phys. Rev. Lett.* **116**, 156402 (2016).
- ⁴⁷ J. Ahn and B.-J. Yang, *Phys. Rev. Lett.* **118**, 156401 (2017).
- ⁴⁸ S. Park and B.-J. Yang, *Phys. Rev. B* **96**, 125127 (2017).
- ⁴⁹ F. D. M. Haldane, *Phys. Rev. Lett.* **61**, 2015 (1988).
- ⁵⁰ Our model is reduced to the Benalcazar-Bernevig-Hughes model^{1,2} by unitary transformation if the mirror symmetries remain³⁹. However, no crystal symmetry is required to realize the second-order topological phases in this model unless the chiral symmetry is broken.
- ⁵¹ X. Zhu, *Phys. Rev. B* **97**, 205134 (2018).
- ⁵² Y. Wang, M. Lin, and T. L. Hughes, *Phys. Rev. B* **98**, 165144 (2018).
- ⁵³ C.-H. Hsu, P. Stano, J. Klinovaja, and D. Loss, *Phys. Rev. Lett.* **121**, 196801 (2018).
- ⁵⁴ N. Bultinck, B. A. Bernevig, and M. P. Zaletel, *Phys. Rev. B* **99**, 125149 (2019).
- ⁵⁵ Z. Wu, Z. Yan, and W. Huang, *Phys. Rev. B* **99**, 020508(R) (2019).
- ⁵⁶ R.-X. Zhang, W. S. Cole, and S. Das Sarma, *Phys. Rev. Lett.* **122**, 187001 (2019).